Confinement in Bending of High-Strength Lightweight Aggregate Concrete Beams

Jelena Zivkovic[1] and Jan Arve Øverli[1]

[1] Department of Structural Engineering, Norwegian University of Science and Technology, NTNU, Trondheim, Norway

Abstract

The use of lightweight aggregate concrete (LWAC) is limited as a mainstream construction material in structural applications due to more brittle post-peak material behavior and uncontrolled crack propagation compared to normal density concrete (NWC). To improve the ductility of LWAC structures, the confinement effect from the transverse reinforcement in conjunction with longitudinal reinforcement was considered. In addition, it was tested the influence of concrete cover. The ultimate compressive strain at peak load was approximately 3.5‰ for all beams, which is like the level expected for NWC. It is possible to increase the ductility of LWAC structures by appropriate reinforcement detailing.

Keywords: Confined lightweight concrete, ductility, transversal reinforcement, longitudinal reinforcement, concrete cover.

1. Introduction

Lightweight aggregate concrete (LWAC) is defined as concrete with an oven-dry density below 2000 kg/m^3 and it normally has a maximum strength of 80 MPa [1–5]. LWAC has been successfully used for structural applications requiring its high strength-to-weight ratio, greater tensile strain capacity, better durability properties, lower coefficient of thermal expansion, and superior heat and sound insulation characteristics (due to air voids in the lightweight aggregate). Lightweight concrete is also a fire-resistant material, but its main advantage is its low weight. This reduces the dead weight of structures and their foundations in areas with low bearing capacities; structures become more seismic resistant because less mass means reduced inertia forces; and the lighter weight and smaller sections of the structural members make for easier handling and transportation of precast elements [6–10]. Nevertheless, the use of LWAC is limited as a mainstream construction material in structural applications due to its more brittle post-peak material behaviour (especially in compression), its uncontrolled cracking, lower ultimate strain and its reduced ductility [7]. In addition, one of the main disadvantages of LWAC is lower ultimate strain followed by uncertainty about structural integrity in post-peak fase. Besides that, LWAC has a much higher price, and production to achieve the desired strength is much more complicated with consuming higher doses of cement, which increases CO_2 emissions compared to the normal density concrete.In design codes the mechanical properties of LWAC are defined by introducing density dependent reduction factors on the NWC properties [4,5].

The ability of a material, cross section, member or structure to sustain large deformations after the peak load without fracture or failure is known as ductility. The deformations can be strains, rotations, curvatures or deflections. Ductility is essential for safety and is a major consideration in the design of structures to ensure the redistribution of forces and avoid brittle failures. To be able to evaluate the ductility of concrete structures we need knowledge of the complete stress-strain curve in compression, including the descending branch [6,7,10]. The ultimate strain at peak load is the governing value for design. After peak load, the concrete cover may spall. However, the post-peak response is important for the evaluation of residual capacity and safety, even where the structure seems to be destroyed. Very little is known about the complete curve for lightweight aggregate concrete. The main reason for this is the difficulty in capturing the post-peak behaviour with conventional techniques, and testing small specimens in compression results in brittle failures with no ductility. When reinforced concrete sections are subjected to large deformation, their ability to carry load depends primarily on the behaviour of confined concrete [8].

It is well known that confinement increases both the ductility and the strength of the concrete. Bending tests of large prisms or beams are required to obtain ductility data for use in modelling. Confinement in concrete structures is achieved by the suitable placement of reinforcement. The effectiveness of confined reinforced concrete members depends on their cross-sectional properties, the stress-strain behaviour of the concrete and steel, the loading rate, and the strain gradient [10–14]. In reinforced concrete, the passive confinement of transverse reinforcement is the most common, and the effect of confinement is also considered in design codes for concrete structures [4]. Some previous research has addressed the flexural behaviour of LWAC beams, focusing on ductility and confinement factors [11–15] of which the influence of transverse reinforcement is reported as the most common. Many researchers have developed theoretical models to include confinement effects [16–17]. However, most of these models do not include Young's modulus of elasticity and none include the Poisson ratio, both of which are lower in LWAC than in NWC. In the literature most studies on confinement effects are performed on columns subjected to axial force. However, strain gradients and shear reinforcement which do not encircle the compression zone do influence the confinement effect [11-18]. Therefore, this study test beams in bending to investigate confinement in the compression zone.

The main objective in this study was to investigate the passive confinement effect of closed links on the ductility of LWAC structures. An experimental programme was set up with six over-reinforced LWAC beams subjected to four-point bending tests to create a constant bending zone between loading points. The test set-up was created with a view to capturing post-peak behaviour in compression. Various beam configurations were investigated to study the effect of stirrup spacing, the thickness of concrete cover, and the amount of longitudinal compressive reinforcement on bending capacity and ductility.

Study is focused on over reinforced LWAC concrete beams (i.e. on beams with a high longitudinal tensile reinforcement ratio) undergoing bending. In general, ductility and confinement are well documented in the literature for structural members undergoing pure compression, but there is only a limited amount of information for structural members undergoing bending that takes into account the effect of stirrups, compression reinforcement, and concrete cover. Furthermore, most existing models for confinement effects in LWAC do not consider the mechanical properties of LWAC that are different from those of NWC. This study therefore also investigates whether these models are applicable for use in the design of LWAC structures. Maximum stresses and strains are calculated with two material models and compared with the experimental results.

2. Experimental programme

2.1 Test parameters

The experimental programme consisted of six reinforced LWAC beams with a constant moment zone of 1 m between loading points. The programme was designed to eliminate the effect of frictional restraint on post-ultimate deformation, which is typical for uniaxial compression tests [7,10]. This testing technique allows lateral expansion of the central zone in all directions and provides testing of the LWAC under multiaxial states of stress to investigate confinement effects. The parameters varied in the testing zone were the stirrup spacing, the amount of compressive reinforcement, and the concrete cover. The experimental programme is given in Table 1.

For all the tested beams the moment (P_m) and shear (P_s) capacities were calculated in accordance with Eurocode 2 [4]. To ensure bending failure in compression, all the beams were governed by share. The beams measured (width x height x length) 210–330 x 550 x 4500 mm. The effective depth was 486mm for all the tested beams. The beams were over-reinforced using 10ø32 in the tensile zone to ensure bending failures occurred by concrete crushing in the compression zone. The concrete cover in the tensile zone was 32mm. All stirrups had diameter 12mm. Outside the testing zone, all the beams had the same stirrups spacing 70 mm, designed to avoid shear failure, see Fig. 1. The tensile reinforcement ratio is 7.8% which is much

higher than normally allowed in design codes and used in practise. [4]. This was to ensure bending failures in compression. In the compressive zone, Beams 1–5 had two longitudinal bars of ø12 mm, while Beam 6 had two longitudinal bars of ø25 mm. Short longitudinal bars of ø8 mm were used in the compression zone to carry the strain gauges. To avoid anchorage failure at the supports, the tensile reinforcement was welded to a steel plate with dimensions 30x30x330mm. Fig. 1 gives the beam geometry and Fig. 2 illustrates in detail the various cross sections and constant moment zones of the beams. All the beams, small samples, cubes and cylinders were cast from the same concrete batch. The beams were demoulded 24 hours after casting and stored in the laboratory at approximately 20 °C under wet burlap covered with a plastic sheet. They were uncovered two days before the testing. Finally, the beams were painted white for easier detection of cracks and prepared for instrumentation. The test age of the beams varied from 37 to 59 days.

To establish the mechanical properties of the LWAC, cubes (100x100x100 mm), cylinders (Ø100x200 mm), and small beams (100x100x1200 mm) were cast to obtain stress-strain diagrams, compressive strengths (for cubes and cylinders), tensile strengths, Young's module of elasticity, and fracture energy. These small specimens were demoulded after 24 hours and stored in water until testing day. Compression tests on cubes and cylinders were carried out continuously, following the time schedule of the beam testing.

Table 1. Test parameters

Beam number	Identification cover stirrup distance	Concrete cover top [mm]	Tension reinforcement	Compression reinforcement	Stirrup spacing [mm]	Stirrup ratio [%]	P_m [kN]	P_s [kN]
1	B1_20_0	20	10ø32	2ø12	-	-	729	840
2	B2_20_200	20	10ø32	2ø12	200	0.53	729	840
3	B3_20_60	20	10ø32	2ø12	60	1.80	729	840
4	B4_20_100	20	10ø32	2ø12	100	1.08	729	840
5	B5_40_100	40	10ø32	2ø12	100	1.08	726	840
6	B6_40_200	40	10ø32	2ø25	200	0.53	800	840

*P_m -calculated moment capacity
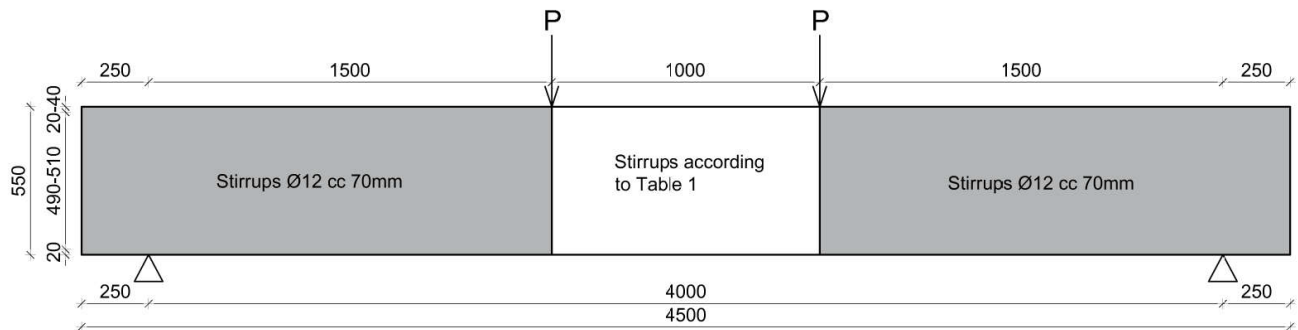
*P_s – calculated shear capacity

Fig. 1 Beam geometry. Dimensions [mm].

2.2 Concrete mix and reinforcement

The concrete mix was prepared from one batch at a concrete stationary plant. Lightweight aggregate was poured into a concrete mixer truck first and then mortar was added. Mixing and transport was carried out in the concrete mixer truck. The lightweight aggregate was North Carolina argillite slate, called Stalite [19]. The argillite slate is a laminated, fine-grained siltstone of clastic rock. The aggregate with an angular shape

3

of the particles is produced by a rotary kiln process. The bulk density ranges from 720–880 kg/m³ for coarse aggregate and 960–1120 kg/m³ for fine aggregate. Toughness of Stalite is determinated following the Los Angeles Abrasion (AASHTO T96) procedure [19,20], and is in the range 25-28.
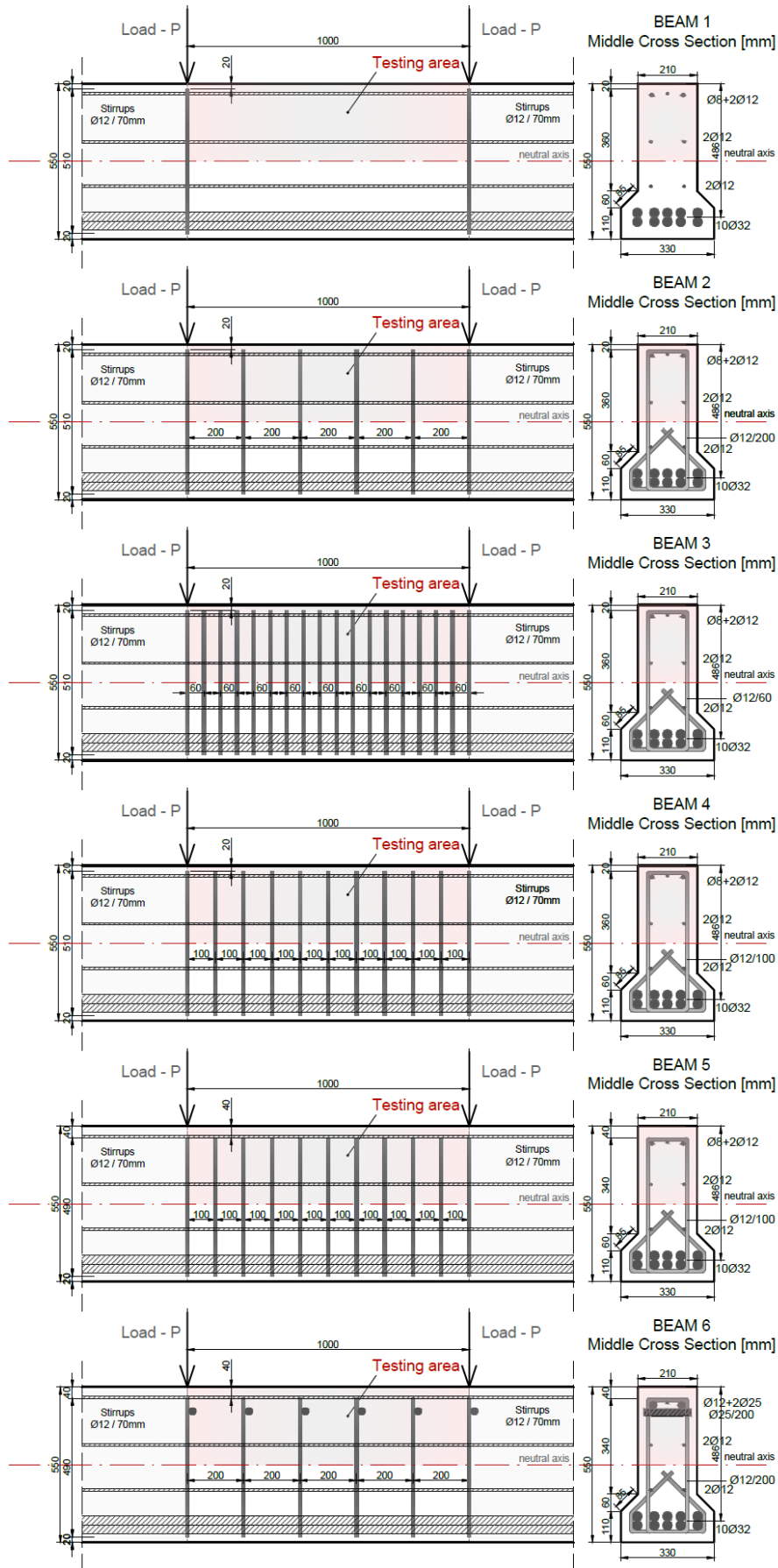
Fig. 2 Testing area with corresponding mid-beam cross section. Dimensions [mm].

With a 24hour water absorption of approximately 6% and relatively high particle strength, concrete containing Stalite can achieve a compressive strength of more than 80MPa.

The moisture content and the water absorbed in the aggregate were measured [9–10]: the moisture was 11.43%, and the absorption after 24 hours and 100 hours was 6.54% and 8.32%, respectively. Table 2 gives the concrete mix recipe. Only the ½" (12.7mm) fraction of Stalite was used. The characteristics of the fresh concrete were density 2013 kg/m^3, air content 2.4%, and slump 230 mm. The reinforcement was of the type B500NC [21]. Its assumed yield stress as used in the calculations was 550 MPa.

Table 2. Concrete mix for LWAC 65

Constituent	Weight [kg/m^3]
Cement (Norcem Anlegg FA)	430.75
Silica fume (Elkem Microsilica)	22.38
Water (free+absorbed 24 hours)	123.33+55.17=178.5
Sand (Ramlo 0–8 mm)	595.31
Sand (Ramlo 0–2 mm)	249.65
Aggregate (Stalite ½")	550
Superplasticizer (Mapei Dynamon SR-N)	5.4

2.3 Mechanical properties

The small beams were tested for facture energy after 71 days. The other small specimens were tested after 28 days to determine their compressive strength, tensile strength and Young's modulus. Table 3 gives a brief summary of the small-scale test results. Based on the cube and cylinder strength at 28 days from Table 3, the concrete corresponds approximately to concrete class LC60 in the design codes [4]. This represents a high-strength lightweight concrete. The compressive failures of cubes and cylinders were very explosive, which is typical for high-strength and lightweight concrete. We determined the fracture energy and characteristic length of the 100x100x1200 mm beams in accordance with SINTEF procedure KS14-05-04123 [24]. These two parameters together characterize the brittleness of concrete. Lightweight concrete with aggregate from Stalite showed a good performance with brittleness comparable with other typical lightweight aggregates and high-strength normal density concrete [25].

Table 3. Material properties for LWAC 65

Saturated density	ρ_{cs} = 2013 kg/m^3
Oven-dry density	ρ_{cv} = 1834 kg/m^3
Compression cube after 7 days	$f_{lcm,7}$ = 56.7 N/mm^2
Compression cube after 28 days	$f_{lcm,28}$ = 74.2 N/mm^2
Compression cylinder	f_{lcm} = 65,1 N/mm^2
Tensile strength	f_{lctm} = 4.03 N/mm^2
Modulus of elasticity	E_{lcm} = 24175 N/mm^2
Fracture energy	G_F = 70,5 Nm/m^2
Characteristic length	l_{ch} = 104 mm

2.4 Test procedure and instrumentation

The load was applied using a mechanical screw jack and transferred to the test beam through a steel spreader beam. Two steel rollers supported the entire width of the beam. The loading points had free rotation

transverse to the beam. Between the jack and the beam surface, a 100 mm wide steel plate and a 15 mm thick fibreboard with the same width was used. Both supports were free to rotate and displace in the longitudinal direction. At the supports, there were only steel plates between the support and the beam. The supports were positioned 250 mm from the beam ends. To avoid anchorage problems, tension reinforcement bars were welded to a steel plate with dimensions 30x60x330 mm. The load was measured under the screw jack using an electrical load cell with a maximum capacity of 2000 kN. Fig. 3 shows the experimental setup and Fig. 4 illustrates the mid-beam cross section with all the measuring devices.
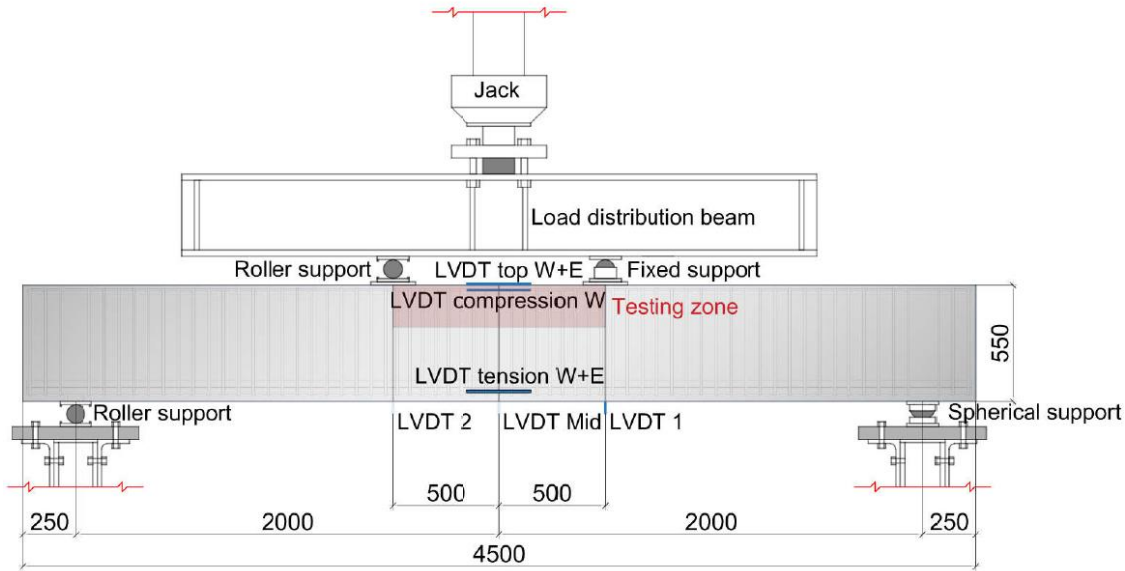

Fig. 3 Experimental set-up of the beam test. Dimensions [mm].
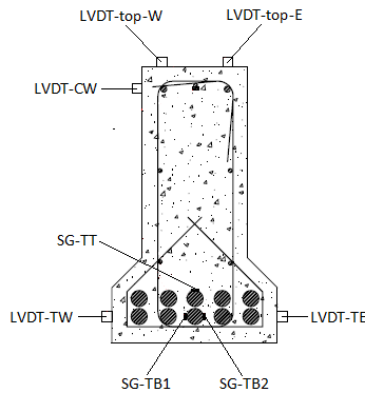

Fig. 4 Mid-beam cross section with measuring devices

To record the strains in the mid-span cross section of the concrete and reinforcement, we used a combination of digital image correlation (DIC) [22, 23], linear variable displacement transducers (LVDTs), and strain gauges (SGs). LVDTs were installed on one side of the beam, while on the other side we used DIC. Three LVDTs, one at the mid-span and two above each loading point, measured the deflections of the beam. Another five LVDTs measured strains in the concrete surface, three of them in the compressive zone and two in the tensile zone. The LVDTs were positioned in the middle cross section and they measured strains over a distance of 200 mm. In addition, six SGs (type FLA-6-11-5L with a gauge resistance of $119.5\pm0.5\Omega$) were inserted on ø8 mm bars in the compressive and tensile reinforcement in the middle cross section.

The load was applied stepwise, with load increments of 100 kN up to 70% of calculated capacity. The load increments were then reduced to 50 kN until failure. The rest periods at each load level were three minutes long and mainly used to draw the crack progression with a dark pen and take photos. The tests were

displacement controlled with a loading rate of 1–1.2 mm/minute; so, the deflection measurements were carried out as a control during all tests. The beams were tested at different ages after casting: 37 days (Beam 1), 50 days (Beams 2 and 3), 55 days (Beam 4), 57 days (Beam 5) and 59 days (Beam 6).

3. Experimental results

3.1 Load displacement relationship

To describe and explain the response of the beams tested, Fig. 5 schematically presents the load-deflection and stress-strain curves of over-reinforced LWAC beams exposed to bending, both with and without confinement. The curves have a peak and several characteristic points that identify the various mechanical stages [15]. The peak load, P_1, with centre point deflection, Δ_1, is defined as the load when horizontal cracking in the compression zone is initiated. When spalling of the concrete cover at the top occurs, the load drops to point C, defined with values $P_{spalled}$ (spalled cross section) and $\Delta_{spalled}$. Due to confinement effects and a deformation-controlled testing system, the load slightly increases to the second peak load level, P_2, with centre point deflection Δ_2. The response can be described by the following stages:

1. 0–A: Before concrete cracks.
2. A–B: Linear response for a cracked section.
3. B–P_1: Nonlinear response and reaching the compressive capacity of the beam, which initiates the spalling of the concrete cover in the compressive zone.
4. P_1–F: Unconfined, very brittle post-peak behaviour.
5. P_1–C: Confined ductile behaviour, the effective cross section is reduced due to spalling and the load drops.
6. C–P_2: Confined ductile behaviour, due to redistribution of the stresses and increasing effective confinement the load goes slightly up reaching a second peak (P_2).
7. P_2–D: Confined ductile post-peak behaviour, the stirrups start yielding, the longitudinal short cracks link together and form an inclined critical crack. The vertical transversal reinforcement bends, and the concrete cover starts to spall from the sides of the cross section. After point D the load continues to decrease before the finale failure occurs.
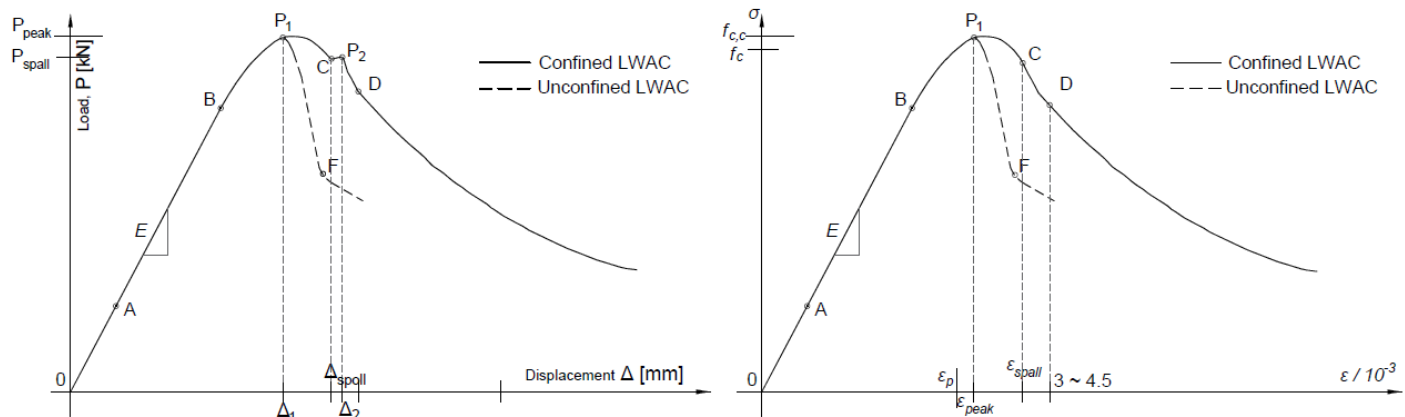

Fig. 5 Characteristic points on the load-displacement and stress-strain curves, with and without confinement

Table 4 gives the test results for the characteristic points shown in Fig. 5. Fig. 6 shows the load-displacement curves for the centre cross sections of the six beams. As expected, Beam 1, without any confinement in the testing area, had a very brittle response after reaching its maximum capacity (load at spalling). The responses for the other beams demonstrated the strong influence of the various confinement configurations on the behaviour at and after spalling. Some increased elastic bending stiffness can be identified where confinement was introduced into the compression gradient zone.

Table 4. Test results

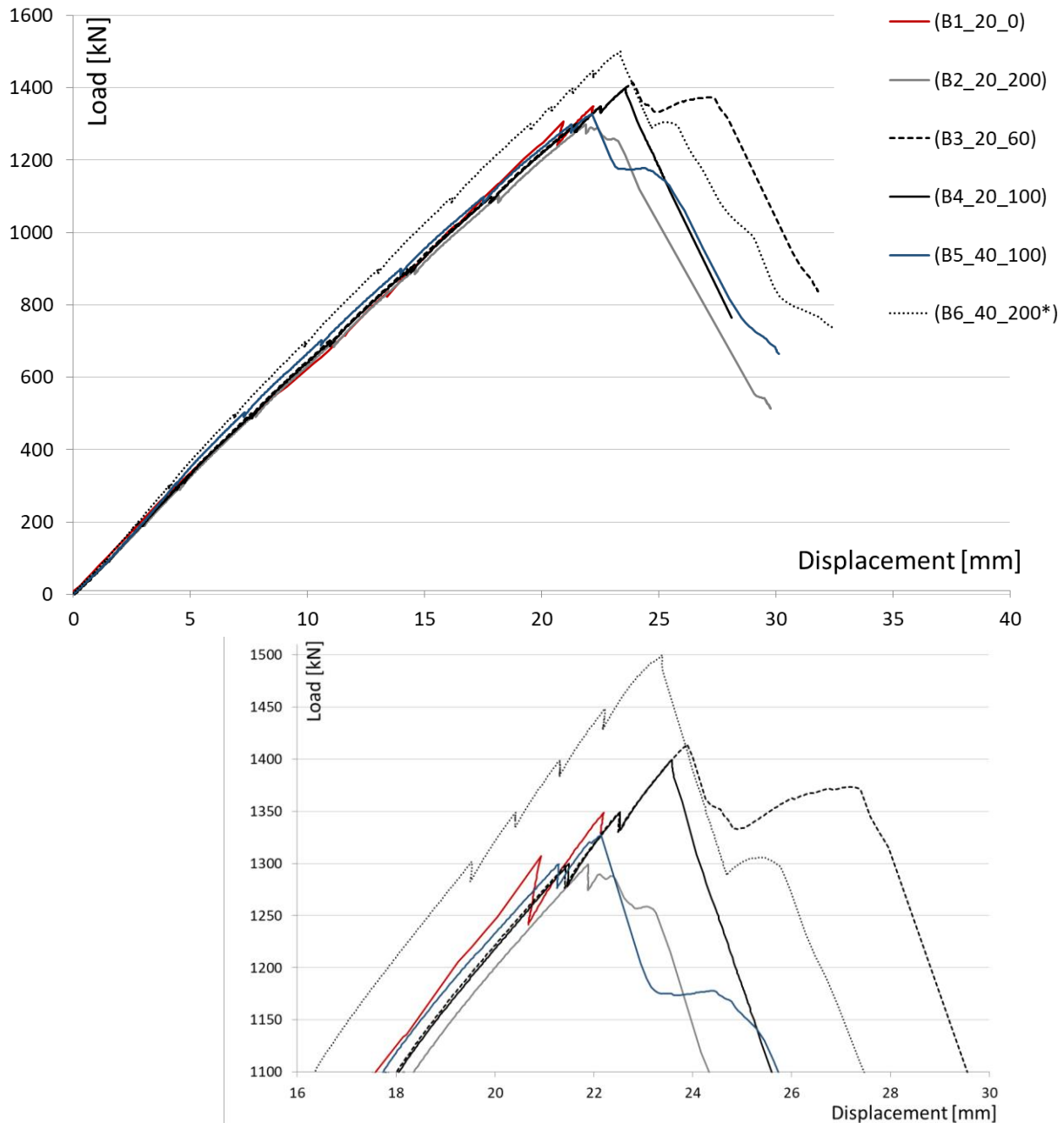| Beams	P_1 [kN]	P_C [kN]	P_2 [kN]	P_D [kN]	$\varepsilon_{c,1}$ [‰]	$\varepsilon_{c,C}$ [‰]	$\varepsilon_{c,2}$ [‰]	$\varepsilon_{c,D}$ [‰]	Δ_1 [mm]	Δ_c [mm]	Δ_2 [mm]	Δ_D [mm]
B1_20_0	675	-	-	-	3.44	-	-	-	22.2	-	-	-
B2_20_200	650	637	645	559	3.75	3.75	3.77	-	21.9	21.9	22.1	29.1
B3_20_60	707	667	687	658	3.74	-	-	-	23.9	24.9	27.2	28
B4_20_100	700	-	-	556	3.75	-	-	5.15	23.6	-	-	25.5
B5_40_100	663	588	589	556	3.61	3.75	3.8	3.8	22.2	23.6	24.4	25.6
B6_40_200	750	644	653	637	3.35	-	-	-	23.4	24.7	25.4	26

Fig. 6 Load-displacement plots (top), with detail of peaks (bottom)

8

All the beams with transverse reinforcement experienced a ductile response. After the initiation of spalling, the load capacity levelled out with no increase in capacity. In the post-peak behaviour, which included a descending branch in the load-displacement response, all the beams had two peaks except Beams 1 and 4. In Beam 4 we notice significant increasing of strains and deflection after peak load, beam didn't show abrupt loss of strength after reach the peak.

The effect of confinement reinforcement can be clearly seen in Fig. 6, where loads and displacements for each beam are given with respect to the spalling load and the corresponding spalling displacement. After the first peak load, the stirrups were able to maintain a cross section, and after some redistribution of the stresses, a second peak point can be identified. All beams experienced very clear unloading after the first peak load, which was associated with the spalling of the concrete cover in the compression zone. For beams with thicker concrete cover, this drop is higher. Overall, the confinement effect from a greater density of stirrups increases both the compressive strength and the ductility. Beam 6, with the most compressive reinforcement, was able to withstand the greatest load and had the largest stiffness.

The experimental investigation showed that the concrete core is effectively confined in compression if it is reinforced with transverse reinforcement with low stirrup spacing ($s \leq 100$ mm, stirrup ratio of 1.08%). This considerably improves and enhances the mechanical behaviour. We also found that the longitudinal compressive reinforcement (A_s) enhances the compressive capacity, but it has less influence on the peak strain and descending curve.

3.2 Failure mode, cracking and ultimate strength and strain

Every beam experienced spalling of the concrete cover in compression between the loading points. Spalling defines the first load peak in the load-deflection curves. The load decreased at this stage for some minutes, before the applied load increased again. The load then continued to increase until the concrete cover in the web started to spall. This defines the second load peak, which is less pronounced. The second spalling resulted in a larger drop in load-bearing capacity and deformations increased fast. It was not possible to increase the load after the second peak and the residual capacity of the beam decreased until the final failure.

Table 5 shows the main parameters and results of the beam tests, where $P_{s.cr}$ corresponds to the force when the first diagonal crack appeared, P_1 is the force of the first load peak, and P_2 the force of the second load peak. The bending capacity ($P_{capacity}$) for all the test beams was calculated in accordance with Eurocode 2 [4]. When calculating the capacity of a beam's compressive strength, its tensile strength, E-modulus and strains in a concrete were multiplied by a density-dependent reduction factor in accordance with the design code [4]. Table 5 also gives average ultimate strains at peak load (ε_{cu}) recorded by two LVDTs located in the compression zone. The average tensile strain (ε_t) represents the two LVDTs located on the bottom side of the beam in the tensile zone.

Fig. 7 shows the cracking of the beams. The first bending cracks observed in the constant moment zone, were at load levels from 25–53 kN. Beam 1, without any stirrups, cracked at the lowest load level. With increasing load, new bending cracks propagated almost symmetrically until they reached the top of the beam flange. Development of the bending cracks almost stopped when shear cracks appeared. The first shear cracks appear in the middle of the shear zone, between the neutral axis and the beam flange. Additional loading led to further crack propagation in both bending and shear areas. The crack propagation for each load step was very similar for all the beams tested.

Table 5 shows that the beams with stiff compressive reinforcement and the most stirrups in the testing area were able to sustain the largest load before the concrete cover began spalling. The compressive longitudinal reinforcement yielded before the first peak load (P_1) in all the beams tested. Spalling of the concrete cover on the sides of the cross section occurred for the second peak load (P_2). This corresponds to the final failure of the beam.
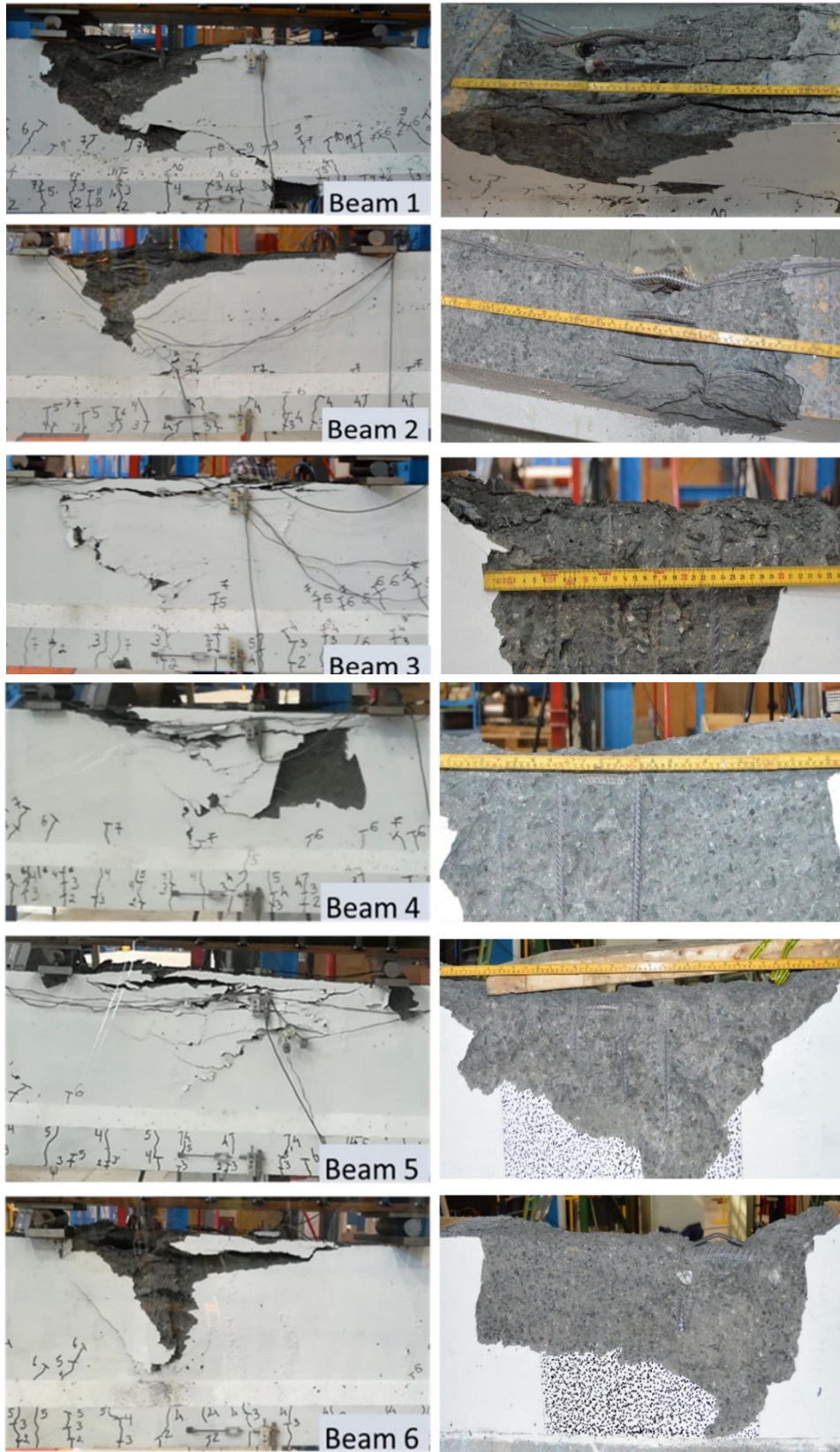
Fig. 7 Cracking and failure in the area between loading points.

Table 5. Test parameters and results

Beams	Cover (c) [mm]	$f_{lc,cube}$ [MPa]	Compress. reinf. (A_s)	Stirrup spacing (s) [mm]	$P_{capacity}$ Calcul. [kN]	$P_{s.cr.}$ [kN]	P_1 [kN]	P_2 [kN]	ε_{cu} [‰]	ε_t [‰]
1	20	75.4	2ø12	-	729	318	675	-	3.44	-
2	20	78.3	2ø12	200	729	350	650	645	3.77	2.04
3	20	78.3	2ø12	60	729	319	707	687	3.74	2.41
4	20	79.4	2ø12	100	729	324	700	-	3.75	2.08
5	40	79.4	2ø12	100	726	339	663	589	3.61	2.17
6	40	79.4	2ø25	200	800	250	750	653	3.40	2.35

Beams with high stirrup spacing and less concrete cover showed earlier spalling and increased crack propagation. When the load applied reached the first peak load, the cross section was reduced due to the spalling of the top concrete cover with the load automatically decreasing. So, beams with thick concrete covers had a greater drop in capacity and the second peak load level was lower. In the final stage, spalling of the web concrete occurred and the load dropped very fast with increasing deformation. Beams with low stirrup spacing can sustain more loading after first peak and they showed a more ductile behaviour. In the beam without stirrups and low concrete cover, a second peak load was not registered. The beam failed immediately after first peak load level. Since all the beams were over-reinforced, tensile reinforcement did not yield at failure, see Table 5. In general, the cracking observed in all the beams tested was very similar to what would be expected in normal weight concrete beams, see Fig. 7. Fig. 7 also shows the importance of stirrup spacing and diameter of the compressive reinforcement on the post peak behaviour. Beam 1 without stirrups experienced buckling followed by a massive spalling of the concrete cover, while Beam 6 with short stirrups spacing and a large diameter did not experience any buckling of the compressive reinforcement.
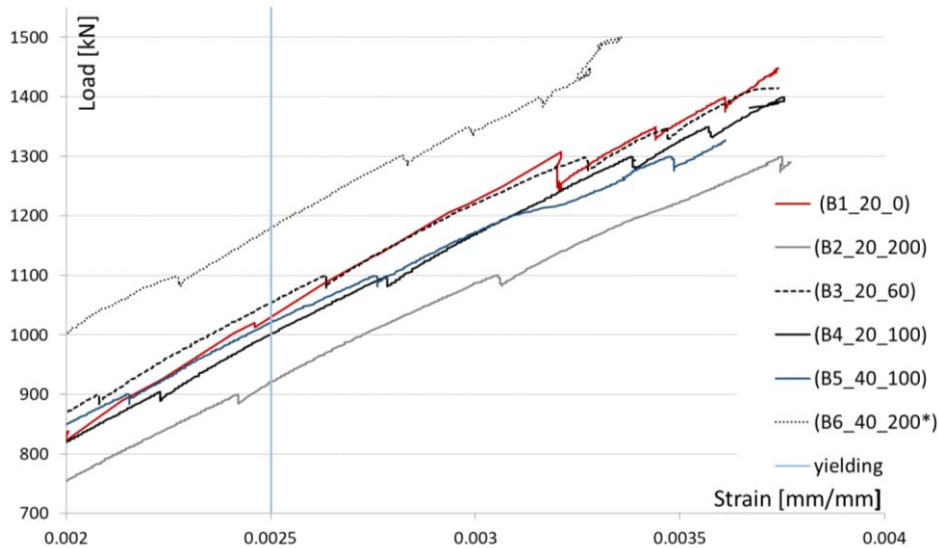
Fig. 8 Average strain in compression at the mid-span versus the total applied load.

By using digital image correlation (DIC), we recorded detailed strain fields of the compressive zones, and in combination with LVDTs, DIC was able to measure strain after spalling of the top concrete cover, see Figs. 9 and 10. We chose a DIC element size of 23 mm to achieve precise and good crack visibility and to optimize time for analysis. Figs. 9 and 10 also show that cables that were part of measuring equipment and sun shadow can disturb DIC analysis, so we have omitted the DIC measurements in these parts of the strain fields. The ultimate compressive strain registered in the beams was in the range of 3.4–3.8‰. Figs. 8–10 and Table 5 show that the strains recorded by LVDTs and DIC were very similar. The detailed strain fields

show the localization of the largest strains in areas prior to failure and that the strain distribution followed the reinforcement detailing. In Beam 6, with the largest compressive reinforcement, high strains were more deeply distributed. The same holds for the thicker concrete cover of Beams 5 and 6, where large strains are clearly deeper and spalling of concrete follows the reinforcement layout, which has also had a clear influence on most of the crack development. Beam 6 exhibited greater stiffness than Beam 4 due to larger amount of compressive reinforcement.
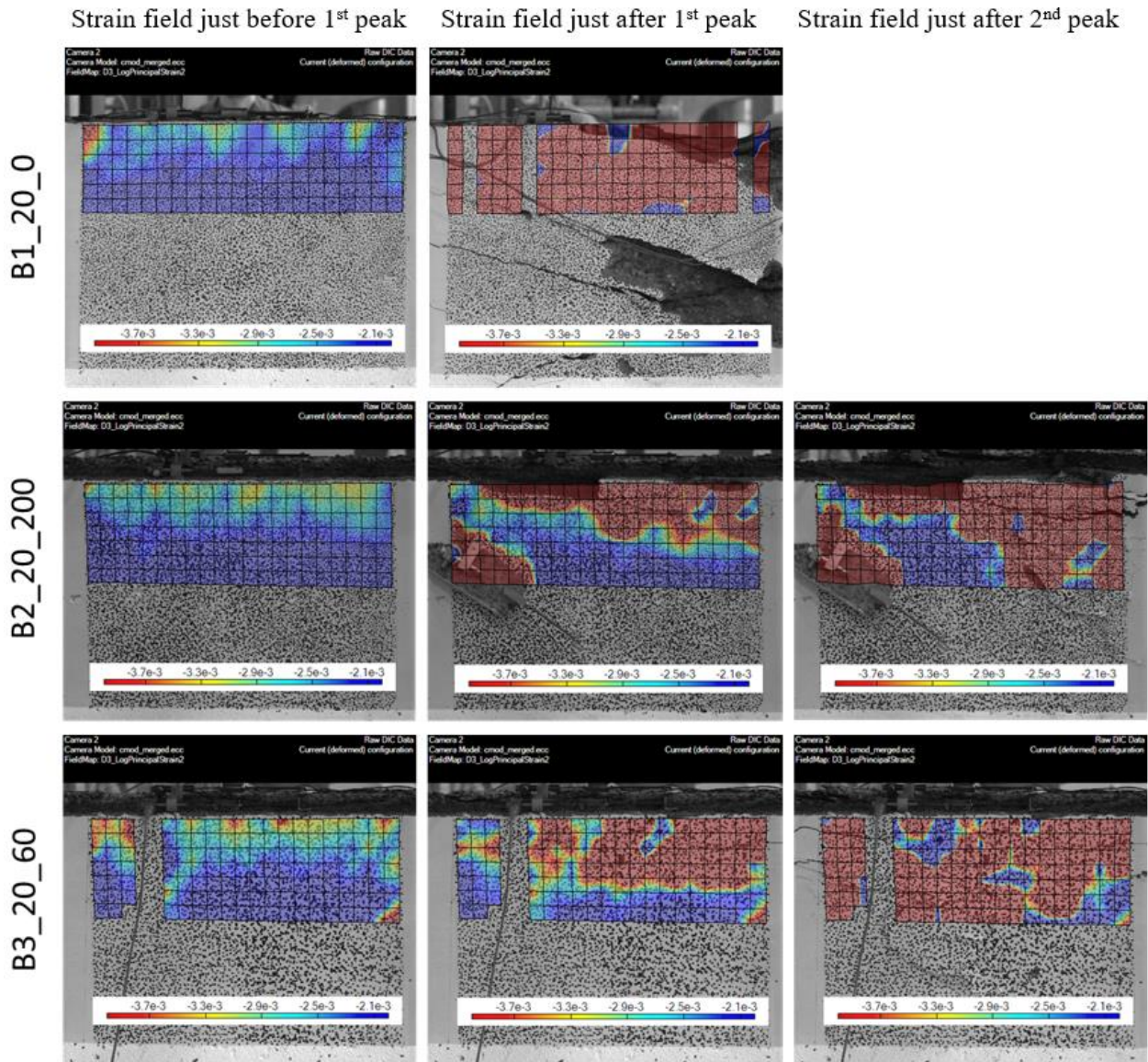

Fig. 9 Strain fields just before and after the 1st peak load level, and after the 2nd peak load level (Beams 1–3).
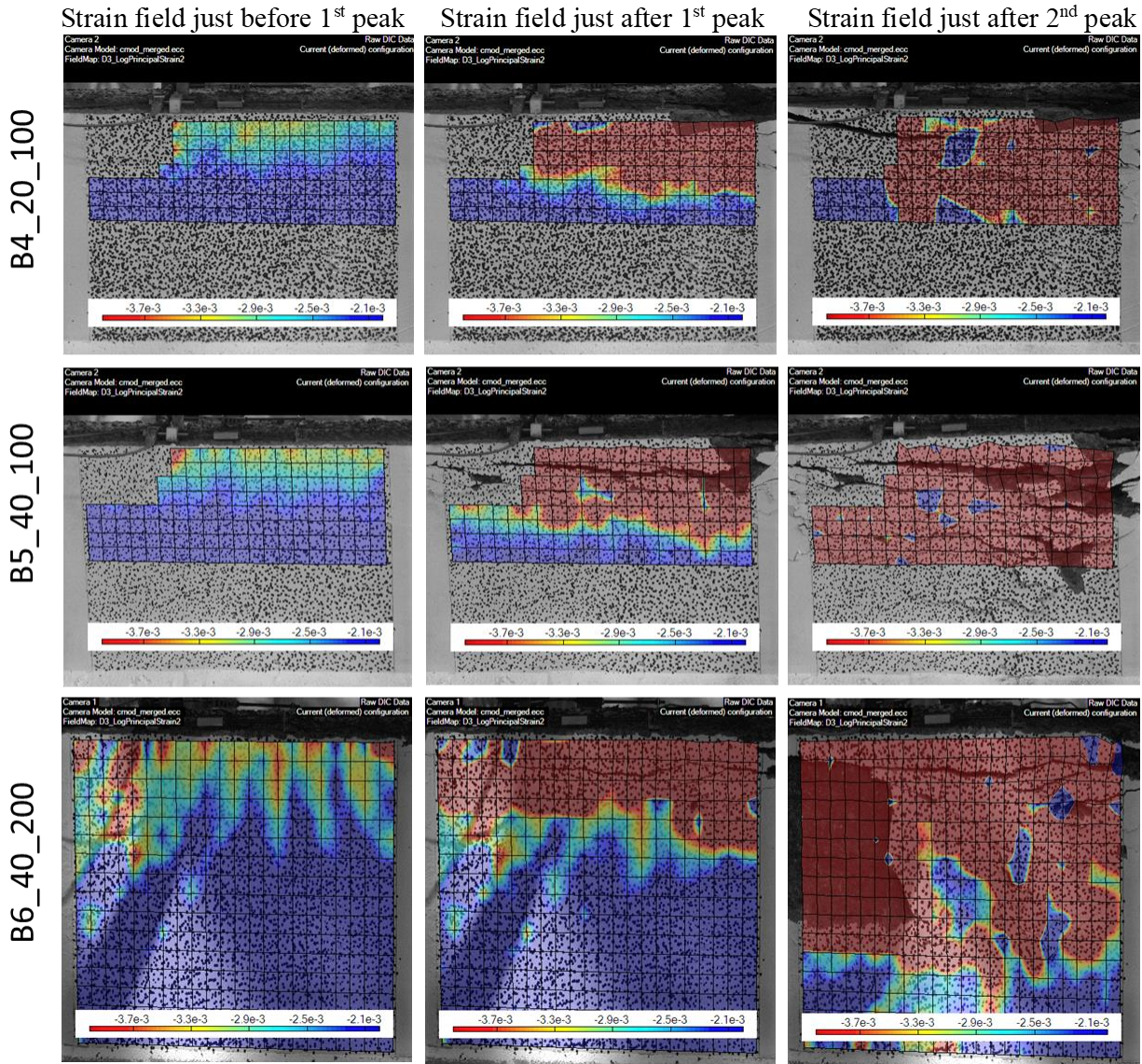
Fig. 10 Strain fields just before and after the 1st peak load level, and after the 2nd peak load level (Beams 4–6).

3.3 Concrete and steel strains

The strain distributions in the beam cross sections for the first bending and shear cracking, at spalling, and at peak load are illustrated for each beam in Fig. 11, assuming linear strain distribution over height.

Up to P_1, the strain measurements showed a reasonable correspondence between SGs, LVDTs and DIC. However, due to spalling of the cover, most of the strain gauges (SGs) on the compressive reinforcement failed, as did the LVDTs on the top of the beam cross sections, so very few measurements are available thereafter and only DIC was able to record the strains. The strain distribution can be considered to be linear over the cross section and constant in the middle 550 mm of the beams. Strains in the reinforcement were local, while strains on the top and bottom surfaces of the beams represent the average strain over a length of 200 mm. DIC measured a strain area with dimensions 380x500 mm and from this area it is possible to extract any strain vector using computational tools [26]. The response from the tensile reinforcement was elastic up to the peak load for all beams, so the beams can be characterized as over-reinforced. The compression reinforcement contributed to the ductility and load capacity of the beams and developed their

full-yield strength at peak load. The thickness of the concrete cover influenced the confinement and ductility after the first peak load, when the height of the compression zone was reduced. The beams with the thicker concrete cover registered a greater peak load, but also a greater drop in load and ductility.
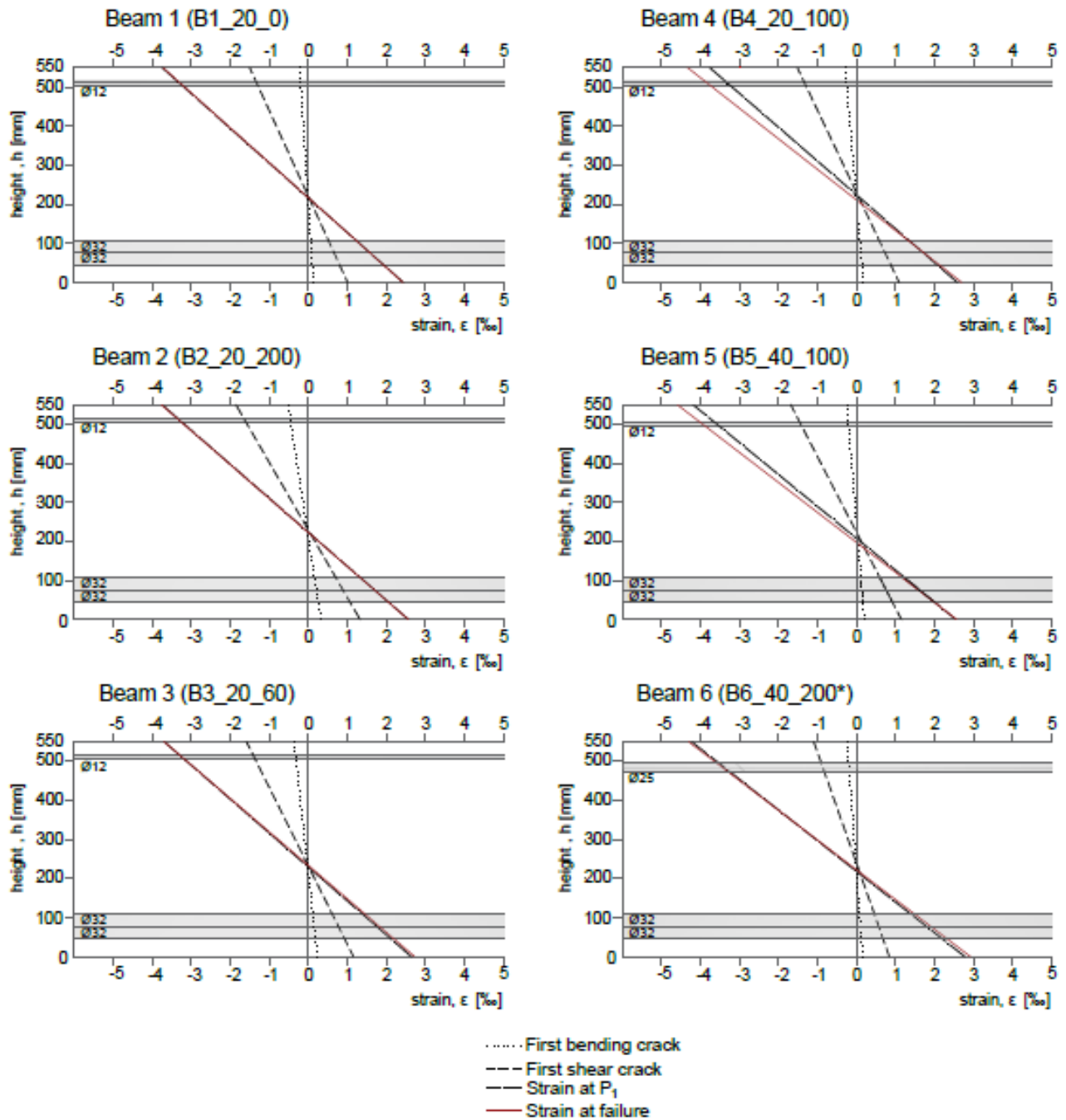

Fig. 11 Longitudinal strain distributions in beam cross sections for first bending and shear cracking, and at spalling and peak load

4. Confined concrete stress-strain model

4.1 General mechanism of rectangular ties (stirrups) in beams

Rectangular, T and I shaped cross sections are widely used in engineering practice. The tie (stirrup) is set up parallel with every edge of a composite rectangular cross section and its main functions are to: form a reinforcement skeleton in combination with longitudinal reinforcement, maintain the correct shape and position during manufacture, carry transverse stress, prevent or reduce the development of longitudinal cracks during service life, reduce the unsupported length of the longitudinal reinforcement, and enhance the ductility.

When a structural member with a rectangular tie is exposed to compression, the straight part of the tie is bent due to expansion of the core. The corner of the tie is stiffer and deforms less, so the core concrete is strongly confined by concentrated compression at its corners and slightly confined by the distributed compression along its edges. The transverse stresses just before failure of the member distribute non-uniformly in the section, see Fig. 12. The confined stresses can be assumed equal ($\sigma_x=\sigma_y$) in elements (1), (5) and (9) along the diagonal line, and they increase towards the corner. However, the confined transverse stresses are different ($\sigma_x \neq \sigma_y$) in the other internal elements (2) and (4). In elements exposed to the outside, the confined stress is mainly one-directional in the direction of the tie in these elements, e.g. σ_x in the elements (7) and (8) and σ_y in the elements (3) and (6). The confined stress in the other direction is less. A compressed beam section can therefore be divided into three zones of different levels of confinement:

1. The zone of non-confinement – concrete cover (outside of the tie);
2. The zone of strong confinement – middle part of cross section with extensions towards the two corners. This zone is under triaxial compressive stress state ($\sigma_x \approx \sigma_y$);
3. The zone of weak confinement – located in the straight parts of the tie. This zone is under biaxial compressive stress state, so the strength enhancement here is limited.
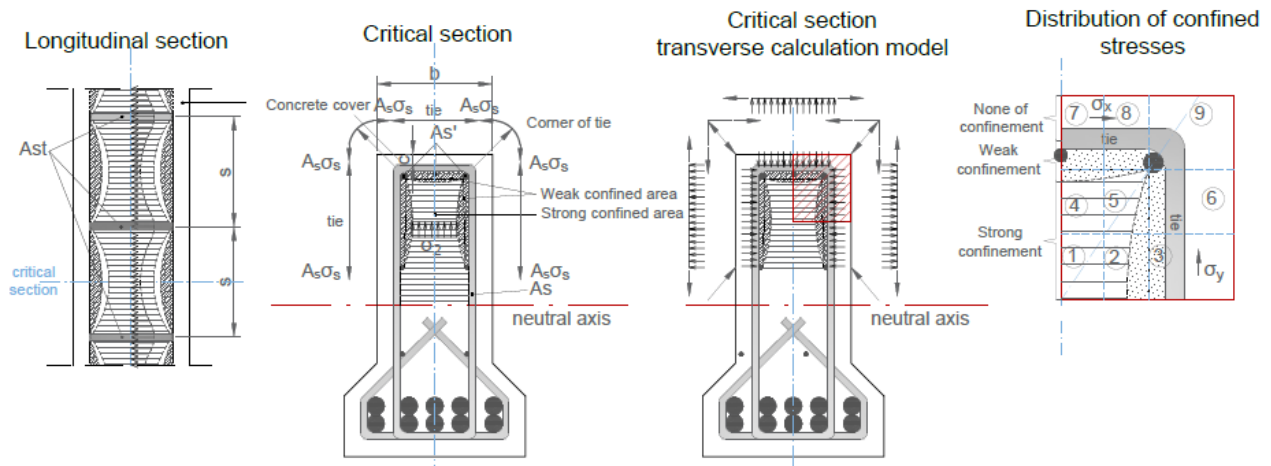

Fig. 12 Rectangular tie (stirrup) – Mechanical analysis and transverse calculation model

Ties are normally set up uniformly, i.e. with the same spacing (s) along the longitudinal axis of the beam. The strongest confinement occurs in the plane of the tie where the zone of strong confinement reaches its maximum. The ultimate strength of the beam is controlled by the weakest section between adjacent ties. With closely spaced ties, the core concrete strength ($f_{c,c}$) and ultimate strain capacity are significantly increased and the ties are able to reach yielding. However, if the spacing of ties is too great, the ties do not yield and the confinement effect for the beam is less. An earlier experimental investigation shows that the confinement is rather small if the spacing of the ties is s > 1–1.5b (where b is the width of the section) [12].

4.2 Confined concrete stress-strain model for tested LWAC beams

Confined concrete is bounded by reinforcement and is under a triaxial compressive stress state, so its strength and deformation ability are greatly enhanced. This is an important measure in engineering practice for improving the mechanical behaviour of a compressive member or part of a structure exposed to compression [12]. A general trend in results from comparison of the various confinement models in the literature is that the peak load, the peak deflection, and the whole ascending branch is accurately predicted by all models [16], whereas the descending branch, or the ductility of confined concrete, is hard to predict and is very often overestimated. So, in addition to the uniaxial compressive strength, the distributions of lateral and longitudinal reinforcement must be parameters in confinement models; the reinforcement ratio is not enough [16–18,27–33].

For comparison, we chose two theoretical models from the literature to validate the results from this experimental study. The first model is the Mander model [17,18], perhaps the best-known and most cited model on confined concrete. In 1984, Mander J.B., Priestly M.J.N and Park R., often identified by the name of the first author listed, proposed a unified stress-strain approach for confined concrete, applicable to both circular and rectangular-shaped transverse reinforcement. Since the model was developed for column applications, some adjustments are needed to apply it to beams. Expressions considering the geometry of beams have been customized in order to calculate the confined concrete area. These assume the concrete in the beam is centrically loaded, as in a column. Reality is somewhat different because, in a beam, there is a stress gradient due to bending. The second confined stress-strain model we employed for comparison was proposed by Bjerkeli and Tomaszewicz and is referred to as the SINTEF model [16,34,35]. It is one of the very few models in the literature tailored for confined LWAC.

Fig. 13 shows a schematic representation of the stress-strain relationship for both models with the main coordinates.
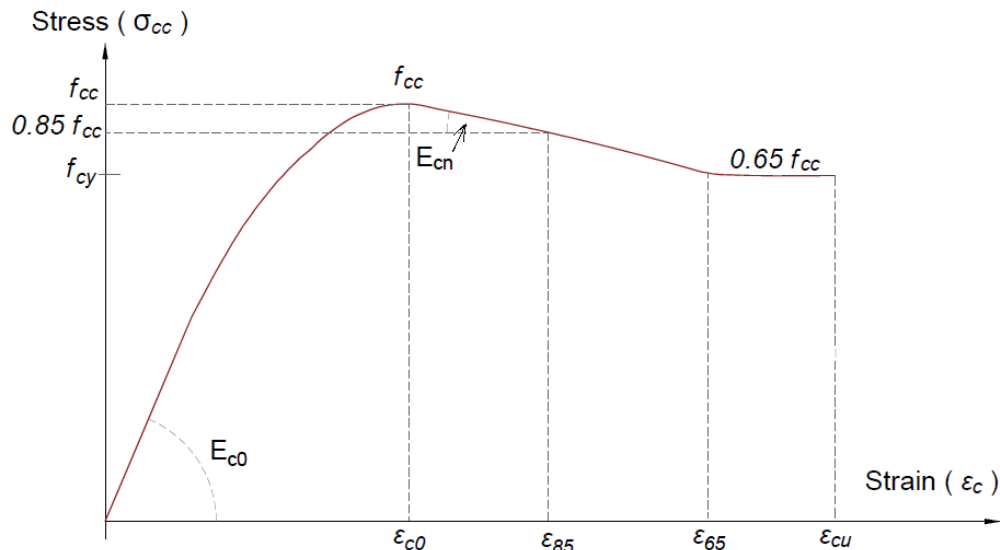

Fig. 13 Stress-strain curve for confined concrete

Both models define three main parts of the stress-strain curve of confined concrete: a parabolic ascending region between zero and maximum stress, a descending linear part between the first and second coordinate, and a horizontal part between the second coordinate and when the concrete reaches its ultimate strain, ε_{cu}. The coordinate $(\varepsilon_{co}, f_{cc})$ corresponds to the peak stress-strain. For the SINTEF model $(\varepsilon_{85}, 0.85f_{cc})$ and for the Mander model $(\varepsilon_{65}, 0.65f_{cc})$ correspond to the representative points of the stress-strain curve after the peak at $0.85f_{cc}$ and $0.65f_{cc}$, respectively. The coordinates $(\varepsilon_{cu}, 0.65f_{cc})$ for the Mander model and $(\varepsilon_{cu}, f_{cy})$ for the SINTEF model correspond to the ultimate strain, as shown in Fig. 13. Equations for the main coordinates are given in Table 6. Based on the uniaxial compressive strength, f_{c0}, the equations contain parameters for confinement stress, geometry, reinforcement configuration, and material properties. Detailed

descriptions of all these parameters can be found in the literature [16–18,34–35]. One important difference between the two models is the density-dependent Young's modulus in the SINTEF model, which makes it suitable for LWAC.

Table 6. Main equations used in the Mander and SINTEF models

Stress-strain curve	Mander model	SINTEF model
Ascending branch $0 \leq \varepsilon_c \leq \varepsilon_{c0}$	$f_{cc} = f_{co}\left(-1.254 + 2.254\sqrt{\left(1 + \frac{7.94 \cdot f_l'}{f_{c0}}\right)} - \frac{2 \cdot f_l'}{f_{c0}}\right)$ $\varepsilon_{co} = \varepsilon \cdot \left[1 + 5\left(\frac{f_{cc}}{f_{c0}} - 1\right)\right]$ $E_{c0} = 11000\sqrt[3]{f_{cc}}$	$f_{cc} = f_{c0} + K_g \cdot 1.5 \cdot f_r$ $\varepsilon_{c0} = 0.0030 + K_g \cdot 0.025 \cdot \frac{f_r}{f_{cc}}$ $E_{cn} = 9500 \cdot \frac{\rho_c}{2400^{1.5}} \cdot f_{c0}^{0.3}$
Descending branch $\varepsilon_{c0} \leq \varepsilon_c \leq \varepsilon_{65}$ $\varepsilon_{c0} \leq \varepsilon_c \leq \varepsilon_{85}$	$\sigma_{cc} = f_{cc} - E_{cn}(\varepsilon_c - \varepsilon_{c0})$ $\varepsilon_{65} = \frac{0.35 \cdot f_{cc}}{E_{cn}} + \varepsilon_{c0}$ $E_{cn} = \frac{6 \cdot f_{c0}^2}{ke \cdot \rho_s \cdot f_{yh}}$	$\sigma_{cc} = f_{cc} - \left(0.15 \cdot \frac{f_{cc}}{\varepsilon_{0.85} - \varepsilon_{co}}\right) \cdot (\varepsilon_c - \varepsilon_{co})$ $\varepsilon_{85} = \left(0.0030 \cdot \left(\left(\frac{12.41}{f_{cc}}\right)^2 + 1\right)\right) + K_g \cdot 0.0025 \cdot \frac{f_r}{f_{cc(1-F)}}$
Horizontal part $\varepsilon_{65} \leq \varepsilon_c \leq \varepsilon_{cu}$ $\varepsilon_{85} \leq \varepsilon_c \leq \varepsilon_{cu}$	$\sigma_{cc} = 0.65 \cdot f_{cc}$ $\varepsilon_{cu} = 0.0035 + 0.4 \cdot \frac{f_l}{f_{c0}}$	$\sigma_{cc} = f_{cy} = 4.87 \cdot \frac{h_c \cdot A_{sh} \cdot f_{sy}}{s_p \cdot A_c}$

Fig. 14 gives the main geometric parameters necessary for the calculation of the confined stress-strain relationships for both the Mander and the SINTEF models. With regard to the cross-sectional geometry, the Mander model reduces the concrete core area for the curvatures that occur when the cross section is cracked, while the SINTEF model considers a flat area bounded by stirrups. Later in the calculation, the Mander model has no reduction factors for the E-modulus and strains to allow for the reduced density of LWAC.

Based on the geometry and reinforcement configuration, the parameters required and calculated in each model are given in Table 7. From the strain distribution recorded during tests (see Fig. 11), the theoretical maximum compressive stress at peak strain was calculated using nonlinear cross-section analysis Two values of maximum stress were found. The first value assumes an unspalled cross section and no confinement effects, as in a regular beam design. The second value takes cover spalling into account and uses a reduced cross section when calculating the maximum compressive stress.

Fig. 15 compares the two theoretical models with the experimentally obtained peak stress and strain points for the unspalled and spalled cross section. Experimental results are obtained from equilibrium using the longitudinal strain distribution from Fig. 11. Both models consider the geometry of a completely confined area. The E-modulus and ultimate strain calculated in the Mander model are overestimated and much greater than in the SINTEF model and the results from our experimental testing. The peak stress was overestimated by both models. The SINTEF model predicted the strain at maximum stress quite well when the beams were confined with transverse reinforcement at spacing s<200 mm. In the cases without or with low confinement (Beams 1 and 2), peak strain was underestimated compared to our experimental results. In tests where stirrups were spaced at 100 mm, the Mander model predicts the strain at maximum quite well, though the calculated ascending branch in all tests is steeper than in the experimental results.
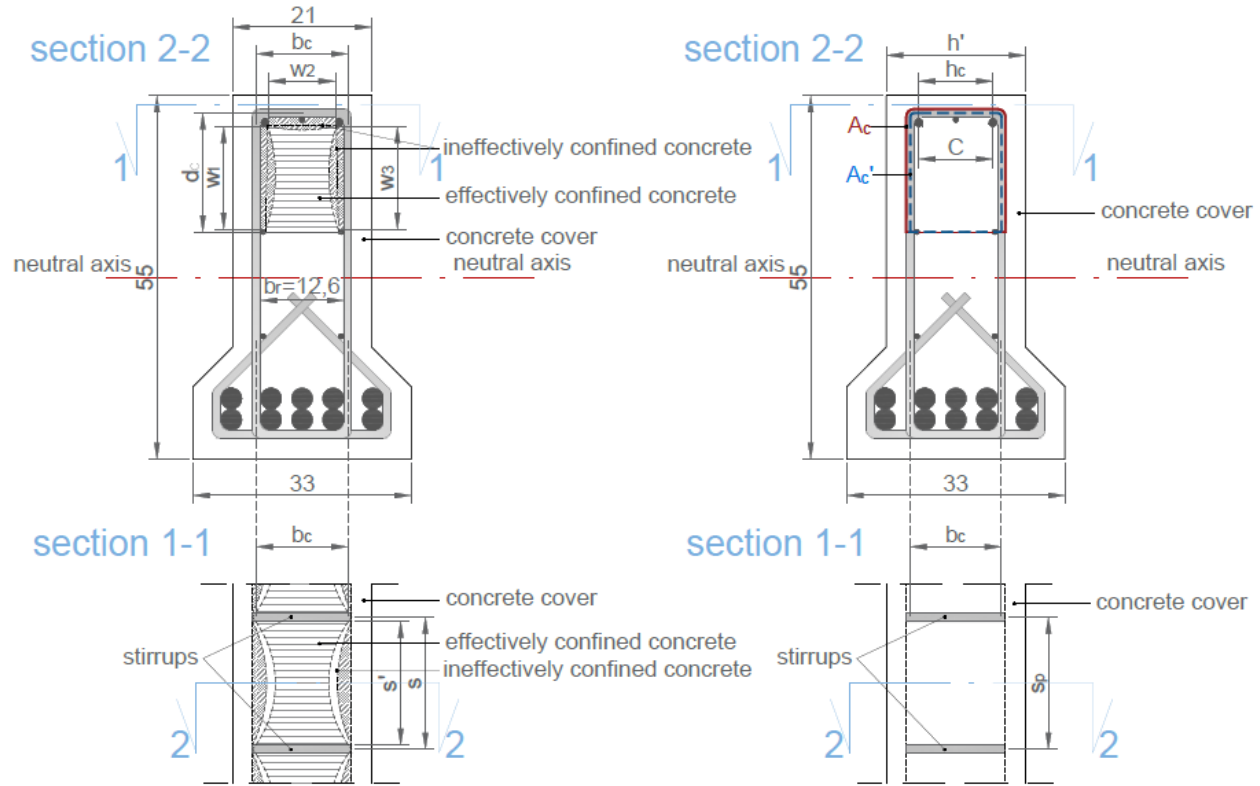
Fig. 14 Section geometry with main parameters for a) the Mander model and b) the SINTEF model

Table 7. Main results using the Mander and SINTEF models

Beams	Mander model					SINTEF model				Calculated stress based on exper. strain distribution	
	f_{cc} [MPa]	E_{cn} [MPa]	ε_{c0} [‰]	ε_{65} [‰]	ε_{cu} [‰]	f_{cc} [MPa]	E_{cn} [MPa]	ε_{c0} [‰]	ε_{85} [‰]	$f_{exp,calc}^{unspalled}$ [MPa]	$f_{exp,calc}^{spalled}$ [MPa]
B1_20_0	65	32500	2	2.7	2.3	56.4	21191	3.02	3.55	41.7	-
B2_20_200	66.8	29343	2.3	3.1	3.8	59.3	21191	3.11	5.58	44.7	76.9
B3_20_60	89.7	15457	5.8	7.8	25.4	67.7	21191	3.36	12.8	49.5	85.4
B4_20_100	76.5	20299	3.8	5.1	12.3	62.9	21191	3.22	8.54	47.5	76.8
B5_40_100	75.9	20640	3.7	5.0	11.7	62.3	21191	3.21	8.36	43.2	67.2
B6_40_200	68.8	26625	2.6	3.5	5.5	59.7	21191	3.12	5.88	49.3	81

In general, the ultimate strain is better predicted by the SINTEF model, while the Mander model underestimates the ultimate strain in cases where the stirrup spacing is at 200 mm or more and overestimates the ultimate strain in cases where the stirrup spacing is at 60 mm (Beam 3).

The SINTEF model showed better agreement with the experimental results. The E modulus, ultimate strain and stress are well predicted and correspond to experimental results, so this model is applicable for the over-reinforced LWAC beams. In the case of large longitudinal compressive reinforcement (Beam 6), both models underestimate the ultimate stress and strain. The Mander model shows good potential because it considers the exact confined cross-sectional area and estimated the stresses and strains for Beams 4 and 5 well, but certain reductions must be introduced into the calculation of the E-modulus. Neither model takes

into account the Poisson ratio, which influences the lateral confinement stresses and is slightly lower for LWAC than for NWC.
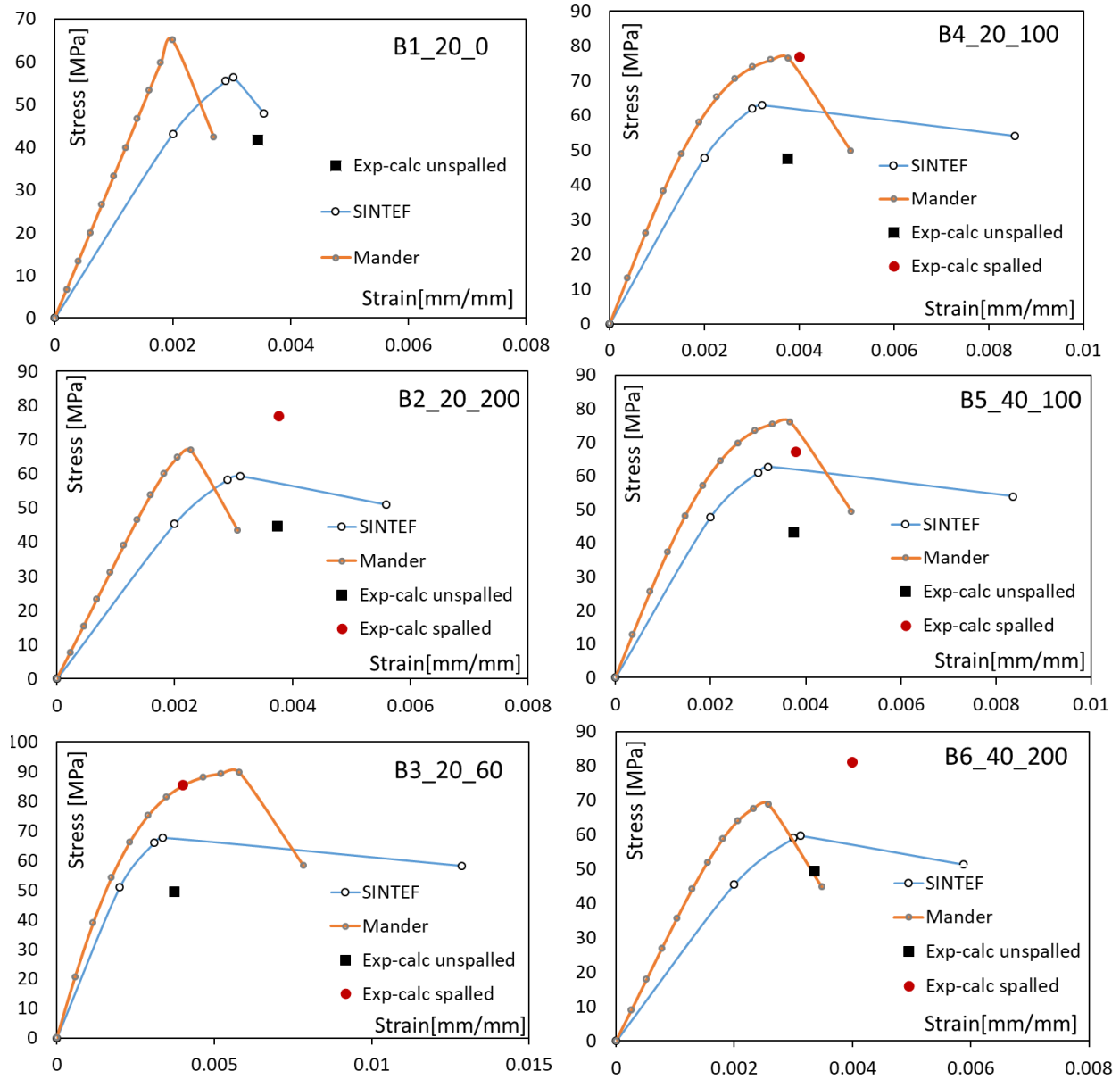

Fig. 15 Stress-strain relationships comparing experimental results with the Mander and SINTEF models

5. Conclusions

The purpose of this study was to investigate the ductility of lightweight aggregate concrete (LWAC) in compression and the influence of various factors on the effectiveness of confinement in compression. The main test parameters were the spacing of transverse reinforcement (stirrups), the amount of longitudinal compressive reinforcement, and the thickness of the concrete cover.

All the beams tested had failure in compression due to a bending moment, followed by spalling of the concrete cover. The beams were able to withstand an increase in load after the formation of shear cracks. Cracking of the beam depended on the test parameters varied in the experiment. Beams with dense stirrup

spacing showed small, shallow cracks and the least spalling. In beams where the concrete cover was thicker, spalling and cracking were greater. The beam containing the largest compressive reinforcement resisted the greatest load. The beam without stirrups in the testing area failed at first peak load level. For the beams with confinement reinforcement, the ultimate compressive strains obtained at peak load were approximately 3.5‰, which is in the same range as expected for NWC.

The results show that introducing various reinforcement configurations significantly affects the post-peak response in the inelastic range of deformation. The use of stirrups or a combination of stirrups and compressive longitudinal reinforcement improved the structural performance with regard to ductility and load-carrying capacity. With reduced stirrup spacing, the ultimate capacity, deflection and ductility increased. Concrete confined with increased longitudinal compressive reinforcement showed the greatest ultimate capacity, but post-peak behaviour was influenced by stirrup spacing. Stirrup distribution provided greater lateral pressure on the compressive zone and therefore greater ultimate compressive strength and ductility. The thickness of the concrete cover did not have a positive effect on ductility; the ultimate load was somewhat greater, but due to reduced confined concrete core, the ultimate strain and ductility were slightly reduced due to greater spalling after the first peak load. The various confinement configurations had no significant effect on the pre-peak response before the initiation of spalling.

We compared our experimental results with two confined concrete stress-strain models: the classical Mander model, and a model proposed by SINTEF which has previously only been published at a conference. The models overestimate the peak stress, and the ascending branch in the models is somewhat steeper than the experimental results. The SINTEF model gives better predictions of ultimate strains and the E-modulus, while the Mander model mostly overestimates these values. However, neither of the models directly includes the Poisson ratio, which influences the confinement since it is slightly lower for LWAC than for NWC.

In general, the strength and ductility of a structural member is a function of the qualities of the LWAC used. This study indicates that it is possible to increase the ductility of LWAC structures by appropriate reinforcement detailing and that LWAC has the potential to comply with the performance requirements for structural materials with regard to ductility in heavily reinforced and post-tensioned structures.

Acknowledgements

References

1. Chandra S, Berntsson L. Lightweight Aggregate Concrete. New York: William Andrew Publishing; 2002.

2. American Concrete Institute. Guide for Structural Lightweight Aggregate Concrete (ACI 213R-03). Farmington Hills, MI, USA: ACI Committee 213; 2003.

3. *fib* Bulletin 8. Lightweight aggregate concrete. Lausanne (Switzerland): International Federation for Structural Concrete; 2000.

4. EN-1992-1-1. 2004. Eurocode 2, Design of concrete structures – Part 1-1: General rules and rules for buildings. Brussels, Belgium: CEN European Committee for Standardization; 2004.

5. NS-EN 1992-1-1:2004+NA: 2008. Eurocode 2: Design of concrete structures – General rules and rules for buildings, Standards Norway; 2008.

6. Nahhas TM. Flexural behavior and ductility of reinforced lightweight concrete beams with polypropylene fiber. Journal of Construction Engineering and Management, 2013;1(1):4–10.

7. Nedrelid, H. Towards a better understanding of the ultimate behaviour of lightweight aggregate concrete in compression and bending. PhD thesis, Norwegian University of Science and Technology; 2012.

8. Holand I, Hammer TA, Fluge F (eds). International symposium on structural lightweight aggregate concrete: proceedings, Sandefjord, Norway. Oslo: Norwegian concrete Association; 1995.

9. Helland S, Holand I, Smeplass S (eds). Second International Symposium on Structural Lightweight Aggregate Concrete: proceedings, Kristiansand, Norway: Norwegian Concrete Association; 2000.

10. Øverli JA. Towards a better understanding of the ultimate behaviour of LWAC in compression and bending. Engineering Structures, 2017;151:821–838.

11. Carmo, RNF, Costa H, Lourenço C, Andrade D Simões T. Influence of both concrete strength and transverse confinement on bending behaviour of reinforced LWAC beams. Engineering Structures, 2013; Vol. 8: 329-341.

12. Guo Z. Principles of Reinforced Concrete: Chapter 9 – Confined Concrete (pp 221–252). Tsinghua, China: Butterworth-Heinemann; 2014.

13. Shah SP, Naaman AE, Moreno J. Effect of confinement on the ductility of lightweight concrete. International Journal of Cement Composites and Lightweight Concrete, 1983;5(1):15–25.

14. Radnic J, Markic R, Harapin A, Matesan D. Effect of confined concrete on compressive strength of RC beams. Advances in Concrete Construction, 2013;1(3):215–225.

15. Jensen TM, Øverli JA Experimental study on flexural ductility in over-reinforced lightweight aggregate concrete beams. SINTEF Building and Infrastructure: COIN Project Report no. 47; 2013.

16. Hansen EA, Tomaszewicz A. Effect of confinement on the ductility of structural members with high strength concrete. SINTEF Report STF65 F90071, 1990.

17. Mander JB, Priestley MJN, Park R. Theoretical Stress-Strain Model for Confined Concrete. Journal of Structural Engineering, 1988;114(8):1804–1826.

18. Mander JB, Priestley MJN, Park R. Observed Stress-Strain Behavior of Confined Concrete. Journal of Structural Engineering, 1988;114(8):1827–1849.

19. Zivkovic J, Castrodale RW, Valum R. Material Properties of High Performance Structural Lightweight Concrete. Paper presented at the Eleventh High Performance Concrete (11th HPC) & the Second Concrete Innovation Conference (2nd CIC), March 6–8, 2017, Tromsø, Norway.

20. AASHTO T 96, Standard Method of Test for Resistance to Degradation of Small-Size Coarse Aggregate by Abrasion and Impact in the Los Angeles Machine, American Association of State Highway and Transportation Officials, 2002, Washington, D.C.

21. NS 3576-3:2012. Steel for the reinforcement of concrete - Dimensions and properties - Part 3: Ribbed steel B500NC.", Standards Norway; 2012.

22. Fayyad TM, Lees JM. Application of Digital Image Correlation to Reinforced Concrete Fracture. Paper to 20th European Conference on Fracture, Procedia Materials Science, 2014;3:1585–1590.

23. McCormick N, Lord JD. Digital Image Correlation for Structural Measurements. Proceedings of the Institution of Civil Engineers – Civil Engineering, 2012;165(4):185–190.

24. SINTEF procedure KS14-05-04123, Fracture energy of prisms with notch in three-point bending test (in Norwegian). SINTEF; 2007.

25. Stemland H. Fracture energy and characteristic length values for Hebron concrete. SINTEF report D6/09-Apr-2012, 2012.

26. Fagerholt E. Accurate measurements of out-of-plane deformations using structured light and close-range photogrammetry. MsC thesis, Norwegian University of Science and Technology; 2004.

27. Popovics S. A Numerical Approach to the Complete Stress Strain Curves for Concrete. Cement and Concrete Research, 1973;3(5): 583–599.

28. *fib*/CEB Bulletin No 197, High strength concrete, a joint FIP/CEB state-of-the-art report, 1990.

29. Bjerkeli L. High-strength concrete. SP1 Beams and Columns. Report 1.1: Ductility of spirally reinforced columns. SINTEF Report STF65 F87040, 1987.

30. Bjerkeli L. High-strength concrete. SP1 Beams and Columns. Report 1.2: Ductility of reinforced small-scale square columns. SINTEF Report STF65 F88051, 1988.

31. Bjerkeli L. High-strength concrete. SP1 Beams and Columns. Report 1.3: Ductility of reinforced large-scale rectangular columns. SINTEF Report STF65 F88068, 1988.

32. Bjerkeli L. High-strength concrete. SP1 Beams and Columns. Report 1.5: Ductility of eccentrically loaded square columns. SINTEF Report STF65 F88068, 1988.

33. Hansen EA. High-strength concrete. SP1 Beams and Columns. Report 1.6: Ductility of over-reinforced beams. SINTEF Report STF70 A93079, 1993.

34. Anwar N, Najam FA. Structural Cross Sections: Analysis and Design. Chapter 6 – Ductility of Cross-Sections (pp 391–481). Butterworth-Heinemann; 2016.

35. Bjerkeli L, Tomaszewicz A, Jensen JJ. Deformation properties and ductility of high-strength concrete. Second international symposium on high-strength concrete, proceedings pp 215–238, Detroit, MI: American Concrete Institute; 1990.